Magnetic properties of the one-dimensional $S = \frac{3}{2}$ Heisenberg antiferromagnetic spin-chain compound $Na_2Mn_3O_7$

Chandragiri Venkatesh,[1] Bilwadal Bandyopadhyay,[1] Arindam Midya,[1] Krishnan Mahalingam,[2] V. Ganesan,[2] and Prabhat Mandal[1]

[1]*Saha Institute of Nuclear Physics, HBNI, 1/AF Bidhannagar, Calcutta 700064, India*

[2]*UGC-DAE Consortium for Scientific Research, University Campus, Khandwa Road, Indore 452001, India*

(Received 12 December 2019; revised manuscript received 2 May 2020; accepted 12 May 2020; published 27 May 2020)

We have performed magnetic susceptibility (χ), heat capacity (C_p), and nuclear magnetic resonance (NMR) measurements on the layered compound $Na_2Mn_3O_7$ in which the magnetic Mn^{4+} ions constitute a maple-leaf lattice. At high temperature, χ follows the Curie-Weiss (CW) law with CW temperature as high as 152 K and Mn^{4+} ions are found to be in the high-spin state ($S = \frac{3}{2}$). With decreasing temperature, χ passes through a broad maximum at 115 K and decreases rapidly at low temperature. A similar broad peak appears at around 62 K in the magnetic contribution to heat capacity (C_m). The temperature dependence of χ and C_m are the characteristics of an one-dimensional Heisenberg antiferromagnetic spin chain with a nonmagnetic ground state. The obtained values of spin-gap energy (Δ_s) and nearest-neighbor antiferromagnetic exchange coupling (J) are 28 and 27 K, respectively. There is no evidence of a long-range magnetic ordering down to 2 K in heat capacity data, in agreement with spin-singlet ground state. These observations are further corroborated by ^{23}Na NMR studies through measurements of both the NMR shift and the spin-lattice relaxation rate.

DOI: 10.1103/PhysRevB.101.184429

I. INTRODUCTION

Low-dimensional antiferromagnets, in particular one-dimensional (1D) spin chains and spin ladders, have been extensively investigated because they exhibit several intriguing physical phenomena such as different types of magnetic ground states for half-integer and integer spin, separation of spin and charge degrees of freedoms, ballistic thermal transport of spinon, etc., that are entirely dominated by the quantum-mechanical behavior and have no three-dimensional analogues [1–8]. Experimental investigations have been devoted mainly to 1D Heisenberg antiferromagnetic (HAF) systems with spin $S = \frac{1}{2}$, as for such spin the quantum effects are more pronounced and the observed results for magnetic susceptibility and heat capacity could be explained with the aid of existing theoretical models [9–12]. Also, theoretical studies indicated that with increasing S, the quantum disordered state is significantly destabilized and a weak interchain coupling may give rise to a three-dimensional magnetic ordering at low temperature [13–15]. Even so, a number of low-dimensional magnetic systems with $S > \frac{1}{2}$ have been studied by various experimental techniques, e.g., magnetization in $Mn(HCOO)_2 \cdot 2H_2O$ ($S = \frac{5}{2}$) [16], $[(CH_3)_4N][MnCl_3]$ [17], $CsVX_3$ and VX_2 halogenides (X = Cl,Br) ($S = \frac{3}{2}$) [18], $AgCrP_2S_6$ [19], 2, 2′-bipyridyl trichloromanganese ($S = 2$) [20], $SrMn(VO_4)(OH)$ ($S = \frac{5}{2}$) [15]; magnetization and heat capacity in $CoSb_2O_6$ ($S = \frac{3}{2}$) [21], 4, 4′-bipyridyl iron trifluoride ($S = \frac{5}{2}$) [14]; inelastic neutron scattering in $CsVCl_3$ and $CsVBr_3$ ($S = \frac{3}{2}$) [22], $RCrGeO_5$ (R = Y or ^{154}Sm) ($S = \frac{3}{2}$) [23]. All the above cited examples belong to linear spin-chain systems.

$Na_2Mn_3O_7$ belongs to the class of recently studied Li- and Na-based manganites that have received considerable interest as electrode materials due to their low-production cost and nontoxicity. In $Na_2Mn_3O_7$, the magnetic Mn ions constitute a two-dimensional maple-leaf lattice. The physicochemical properties of this compound have been studied in the context of application as an electrode material for Na-ion batteries, but there are no reports on its magnetic properties [24–27]. In this work, we have tried to elucidate the nature of the magnetic ground state of $Na_2Mn_3O_7$ by means of dc magnetization, heat capacity, and ^{23}Na nuclear magnetic resonance (NMR) measurements. Our study reveals that in $Na_2Mn_3O_7$, Mn^{4+} ions are in high spin state ($S = \frac{3}{2}$), and remarkably, the spin arrangement yields properties similar to 1D Heisenberg spin chains with antiferromagnetic interaction and a gap in spin excitation spectrum.

II. SAMPLE PREPARATION AND CHARACTERIZATION

The studied compound $Na_2Mn_3O_7$ was synthesized by conventional solid-state reaction method. Na_2CO_3 and $MnCO_3$ powders were mixed in a stoichiometric ratio 1:3 and heated at 600 °C for 10 h. The product was reground, pressed into pellets and sintered at 700 °C for another 4 h in oxygen atmosphere and then the temperature was decreased slowly to 500 °C and kept constant for 10 h, followed by slow cooling. The oxygen atmosphere was maintained during the entire cooling process. Phase purity and the structural analysis were performed at room temperature in a high-resolution x-ray diffractometer (Rigaku, TTRAX III), using Cu-K_α radiation ($\lambda = 1.5418$ Å). The Rietveld refinement was made for the

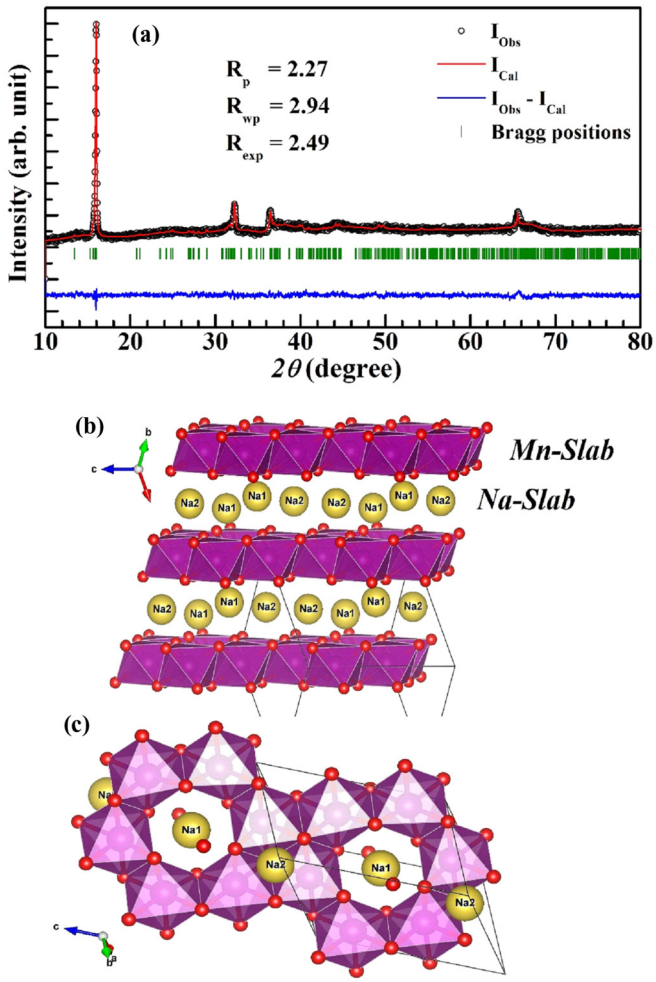

FIG. 1. (a) Room-temperature x-ray diffraction pattern for polycrystalline powder of $Na_2Mn_3O_7$. The parameters for the best-fit results obtained from the Rietveld refinement are also shown. (b) The schematic representation of $Na_2Mn_3O_7$ crystal structure. The two-dimensional layered arrangement of MnO_6 polyhedral sheet is separated by the nonmagnetic Na layer. (c) The arrangement of magnetic Mn^{4+} ion within the MnO_6 octahedra. Na ions are located at two different crystallographic positions.

structural analysis of diffraction pattern of powdered sample with FULLPROF software. Figure 1(a) shows the powder x-ray diffraction pattern. The observed peaks in the diffraction pattern have been indexed with triclinic unit cell having $P\bar{1}$ crystallographic symmetry. Within the x-ray resolution, we have not observed any peak due to the impurity phase. The calculated lattice parameters are $a = 6.6131$, $b = 6.8432$, $c = 7.5405$ Å, $\alpha = 105.57°$, $\beta = 106.01°$, and $\gamma = 111.33°$. The lattice parameters are in good agreement with the earlier reports [27,28]. We have also determined Mn-Mn bond distances and Mn-O-Mn bond angles, which are shown in Table I. The experimental x-ray intensity profile along with the theoretical fit and the Bragg positions are shown in Fig. 1(a). The crystal structure of $Na_2Mn_3O_7$ is shown in Fig. 1(b). $Na_2Mn_3O_7$ has a layered crystal structure with $[Mn_3O_7]_{2-\infty}$ layers built up with edge-sharing MnO_6 octahedra. These layers are separated by Na ions located at two different crystallographic positions and form honeycomblike structures, in which one of the Mn sites is vacant due to the missing of $\frac{1}{7}$ Mn^{4+} ions. The edge-sharing MnO_6 units are arranged in plane with the c axis with Mn atoms located on the sites of maple-leaf lattice and well separated by the alternatively linked NaO_5 and NaO_6 polyhedra, setting a suitable example for the two-dimensional Mn^{4+} maple-leaf spin lattice, as shown in Fig. 1(c). The magnetization measurements were performed using a Superconducting Quantum Interference Device-Vibrating Sample Magnetometer (MPMS 3, Quantum Design). The heat capacity (C_p) measurement was performed by relaxation method using a physical property measurement system (Quantum Design) and the data were recorded in the temperature range 1.8–350 K. Nuclear magnetic resonance measurements were performed with a Bruker 300 MHz Ultrashield magnet, Thamway PROT4103MR spectrometer and a cryostat of Oxford Instruments. The last one houses the homemade NMR sample rod that has tuning and matching capacitors, and a cernox temperature sensor in proximity with the rf sample coil. The spectra at various temperatures between 4 and 296 K were recorded by the process of integration of spin-echo signals while sweeping the rf in 20 kHz steps over the position of ^{23}Na resonance using a $\frac{\pi}{2}$-τ-$\frac{\pi}{2}$ solid echo pulse sequence. The spin-lattice relaxation time measurements were performed at the peak of the resonance spectrum using the saturation recovery method.

III. RESULTS AND DISCUSSIONS

A. Description of Hamiltonian

The generic form of the Hamiltonian for a given Heisenberg antiferromagnetic lattice akin to the triangular arrangement of spins can be written as,

$$H = \sum_{\langle i,j \rangle} J_{ij} S_i . S_j, \tag{1}$$

in which J_{ij} runs over the nearest-neighbor sites. This Hamiltonian was utilized to describe the possible long-range ordering in the $S = \frac{1}{2}$ maple-leaf lattice [29]. The maple-leaf lattice could be treated as a unit cell of hexagon running through spin sites in six triangular lattices and the above-mentioned Hamiltonian [Eq. (1)] becomes,

$$H = J \sum_{\langle i,j;m,n \rangle} S_i^m . S_j^n. \tag{2}$$

Here, J spans among the equivalent magnetic sites, while the spin operators have been taken through each triangular spin lattice site with $n, m = 1, 2, 3, 4, 5, 6$. The three spins that connect to each triangular lattice form a Néel state with 120° rotated spins and the Hamiltonian contains a unique value of J as the maple-leaf lattice has the undistorted triangular Bravais lattice. However, in case of $Na_2Mn_3O_7$, the XRD data refinement results show a strong lattice distortion, as a consequence, there are three distinguishable Mn sites in the Mn_3O_7 layer, viz., Mn1, Mn2, and Mn3, as shown in the schematic diagram (Fig. 2). We have used the same notation to represent the multiple J as in the case of the earlier work on $MgMn_3O_7.3H_2O$ system [30]. J_d lies along the dimer bond between the two Mn sites while the other one, J_t, forms the

TABLE I. The Mn-Mn bond distances and bond angles (Mn-O-Mn) extracted from the Rietveld refinement of $Na_2Mn_3O_7$ XRD pattern and their corresponding exchange interaction (notations taken from Ref. [30]).

J type	Bond	Mn-Mn distance (Å)	Mn-O-Mn angle(°)	
J_{d1}	Mn3-Mn3	2.6417	Mn3-O5-Mn3	–
			89.97	
J_{d2}	Mn2-Mn2	2.6565	Mn2-O2-Mn2	–
			89.98	
J_{t1}	Mn2-Mn1	2.9448	Mn2-O2-Mn1	Mn2-O3-Mn1
			102.95	95.06
J'_{t1}	Mn2-Mn1	2.5837	Mn2-O2-Mn1	Mn2-O4-Mn1
			90.19	87.56
J_{t2}	Mn3-Mn2	2.9742	Mn3-O5-Mn2	Mn2-O7-Mn2
			107.32	91.45
J_{h1}	Mn1-Mn1	3.0359	Mn1-O1-Mn1	–
			97.73	
J_{h2}	Mn3-Mn1	3.2106	Mn3-O1-Mn1	Mn3-O6-Mn1
			96.47	111.83
J'_{h2}	Mn3-Mn1	2.9964	Mn3-O1-Mn1	Mn3-O4-Mn1
			91.05	105.39

triangular lattice bonds and the third one, J_h, establishes the sides of hexagon that connects these triangular spin sites. Furthermore, as a result of lattice distortion, J_d splits into two components (J_{d1}, J_{d2}); J_t splits into three components (J_{t1}, J'_{t1}, J_{t2}); and J_h splits into three components (J_{h1}, J_{h2}, J'_{h2}). The calculated Mn-Mn bond lengths and Mn-O-Mn bond angles and their corresponding exchange interactions are given in Table I.

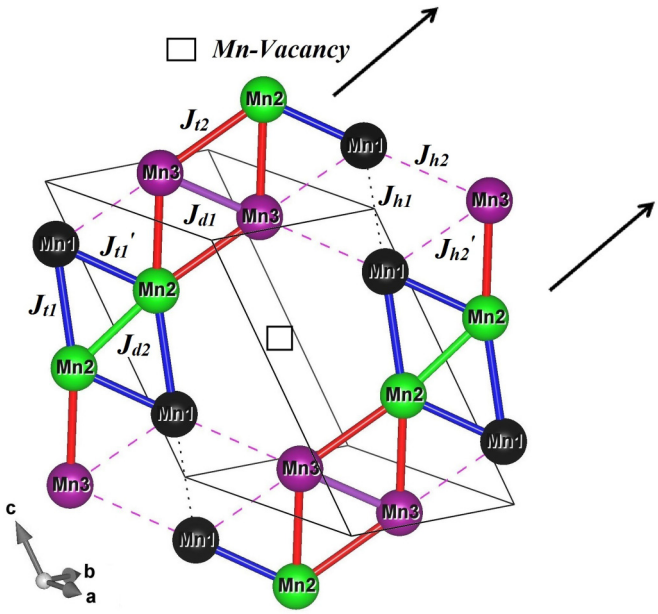

FIG. 2. The schematic diagram of the distorted Mn_3O_7 layer containing three different Mn sites (oxygen atoms are not shown). The blue color bonds indicate exchange couplings of J_{t1} and J'_{t1} (bond distance of J_{t1} is greater than J'_{t1}); the red color bond has exchange coupling of J_{t2}; the violet color bond has exchange coupling of J_{d1}; the green color bond has exchange coupling of J_{d2}; the dashed bonds have exchange coupling of J_{h2} and J'_{h2} (bond distance of J_{h2} is greater than J'_{h2}) and the dotted bond has exchange coupling of J_{h1}. The black arrows indicate the quasi-1D behavior of Mn-Mn bond pairs or Mn-Mn bond trimers running diagonally with respect to the three crystalline axes. The square box represents the depleted location of the Mn atom to form maple-leaf lattice with the remaining six Mn atoms.

Hence, the Hamiltonian could be rewritten as,

$$H = \sum_{\langle i,j;m,n\rangle} J_{ij} S_i^m . S_j^n, \tag{3}$$

where i, j run over the nearest-neighbor sites. Taking into account all the different Mn-Mn bonds within the unit cell, the expandable form of the above Hamiltonian can be written as,

$$\begin{aligned} H = &-2J_{h1}S_1.S_2 - 4J_{t1}S_1.S_2 - 4J_{t1}{}'S_1.S_2 - 2J_{h2}S_1.S_3 \\ &- 2J_{h2}{}'S_1.S_3 - 2J_{d2}S_2.S_2 - 8J_{t2}S_2.S_3 \\ &- 2J_{d1}S_3.S_3, \end{aligned} \tag{4}$$

where S_1, S_2, and S_3 are the respective spin vectors at Mn1, Mn2, and Mn3 sites. The superexchange interaction via Mn^{+4}-O-Mn^{+4} competes with the direct exchange among the t_{2g} orbitals [31,32]. For $MgMn_3O_7.3H_2O$, it was considered that $J_d \gg J_t > J_h$, and $J_h \sim 0$ [30]. In the present case also, as indicated by the structural data in Table I, the above mentioned inequality is valid, i.e., the relative strengths of J_d components, and J'_{t1} are much higher with respect to J_h and other J_t components. This leads to quasi-one-dimensional spin chains made of zigzag strong and weak exchange interactions and aligned in the direction as shown by the arrows in Fig. 2.

B. Magnetic susceptibility

Figure 3(a) shows the temperature dependence of static magnetic susceptibility ($\chi = M/H$) for $Na_2Mn_3O_7$ in the range 1.8–350 K with an applied field of 2 kOe. χ exhibits a nonmonotonic temperature dependence. With decreasing temperature, χ increases and passes through a maximum around 115 K. The broad nature of susceptibility maximum is a characteristic feature of short-range spin correlation. Upon further

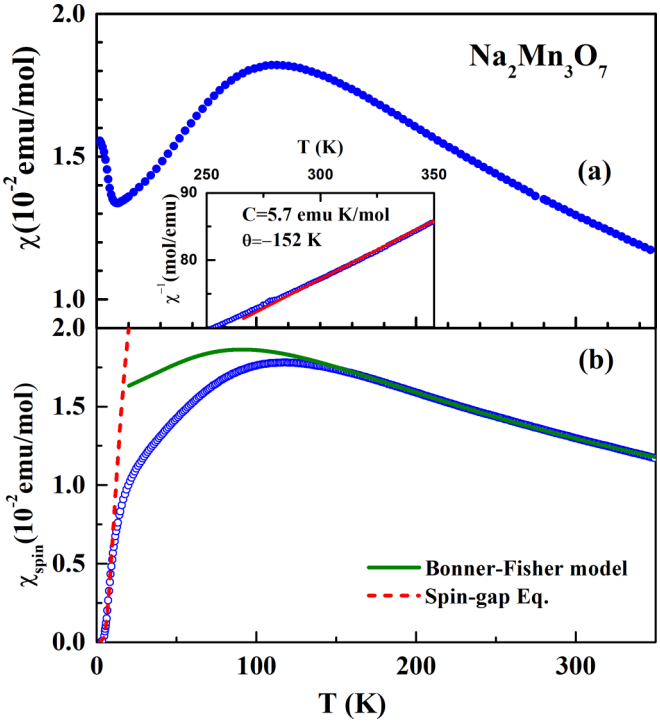

FIG. 3. The top panel (a) shows the temperature dependence of measured magnetic susceptibility (χ) of $Na_2Mn_3O_7$ in the temperature range 1.8–350 K and for an applied field of 2 kOe (•). The inset of top panel shows the inverse of the corrected susceptibility data, χ_{spin}, as a function of temperature and the red solid line is the linear fit to the data with the Curie-Weiss law in the temperature range 280–350 K. In the bottom panel (b), χ_{spin} is shown in the temperature range 1.8–350 K (○). The red dashed and green solid lines are fitted to χ_{spin} with the Bonner-Fisher model [Eq. (5)] at high temperature and with the spin-gap susceptibility [Eq. (7)] at low temperature, respectively, as described in text.

cooling, $\chi(T)$ exhibits an upturn below 10 K, attributable to the paramagnetism of defects and a low concentration of spins of isolated Mn^{4+} ions, which is quite common in such a low-dimensional system [33–38]. In order to determine the contributions of isolated Mn^{4+} spins and atomic cores, the low-temperature part of χ is fitted with the Curie-Weiss (CW) expression, $\chi_d = \chi_0 + C_{LT}/T$, where χ_0 represents the temperature-independent Van Vleck paramagnetic term plus the diamagnetic contribution from the atomic cores. χ_d is subtracted from the measured χ to obtain the true value of the spin susceptibility, χ_{spin}, of the system. In Fig. 3(b), χ_{spin} plotted as a function of temperature shows that χ_{spin} is essentially the same as χ above 50 K and the position of maximum shifts slightly toward higher temperature, at $T_{max} =$ 118 K.

At high temperature well above the maximum, χ_{spin} can be fitted again with the CW expression, which may be written as, $\chi_{spin} = C/(T - \theta_{CW})$, where C is the Curie constant and θ_{CW} is the CW temperature. Inset of Fig. 3(a) shows the linearity of χ_{spin}^{-1} with T above 275 K. This analysis yields $C = 5.7$ emu K/mol, which corresponds to $S = \frac{3}{2}$, the spin only moment of Mn^{4+} ion in the high-spin state. The fit also reveals a very high CW temperature, $\theta_{CW} = -152$ K. The negative CW temperature confirms the existence of antiferromagnetic exchange interaction between the Mn^{4+} ions. In spite of such a high value of θ, the system does not undergo a long-range magnetic ordering at low temperature down to 1.8 K, indicating very weak interchain interaction. A more general expression such as modified Bonner-Fisher model for linear spin chains can be used to describe the nature of high-temperature susceptibility [15],

$$\chi_{spin} = C/T\left[\frac{1+U(q)}{1-U(q)}\right], \tag{5}$$

$$U(q) = cothq - \frac{1}{q}; \quad q = \frac{2JS(S+1)}{k_BT}, \tag{6}$$

where J is the nearest-neighbor antiferromagnetic exchange coupling along the chain and is defined through the Hamiltonian $H = 2J\Sigma S_iS_{i+1}$. We have used the value of C deduced from the high-temperature CW behavior of χ_{spin}. The fit to the susceptibility data is shown in Fig. 3(b). It is clear from the figure that χ_{spin} fits with the Bonner-Fisher model over a much wider temperature range as compared to the CW expression. From the best-fit analysis of the data, we deduce $J/k_B = 27$ K. The position of the maximum of $\chi_{spin}(T)$ curve has been numerically calculated as a function of J for different values of spins. For an 1D HAF spin chain with $S = \frac{3}{2}$, the relation between T_{max} and J, $k_BT_{max} = 4.75J$, yields the value of J about 25 K [39]. Thus the values of J calculated using two independent methods are close to each other.

At low temperature well below the broad maximum, the susceptibility decays exponentially due to the opening of a gap (Δ_s) in the spin excitation spectrum. The value of the spin gap can be estimated by analyzing the low-temperature part of the $\chi_{spin}(T)$ curve using the expression for susceptibility of a gapped 1D spin chain. The magnon dispersion can be approximated to the quadratic form $\varepsilon(k) = \Delta_s + v^2k^2/2\Delta_s$ and in the low-temperature limit ($k_BT < \Delta_s$), χ_{spin} can be fitted with an exponential relation [40,41],

$$\chi_{spin} \propto \left(\frac{\Delta_s}{T}\right)^{1/2} \exp(-\Delta_s/k_BT). \tag{7}$$

Below 15 K, χ_{spin} fits well with the above expression, indicating a predominantly one-dimensional character of the magnetic interactions and a nonmagnetic ground state. The fit yields a Δ_s of about 28 K. This value of spin-gap energy is comparable with that reported for several other integer spin 1D systems [36,37]. It may be mentioned here that an isotropic 1D HAF spin chain with nearest-neighbor interaction yields a gapless spin excitation spectrum for $S = \frac{3}{2}$ [42,43]. However, several half-integer HAF spin chains with nonuniform exchange interactions, as is the case for the present compound, have also shown finite spin gap [23,44–48]. Theoretically, alternating bond $S = \frac{3}{2}$ 1D spin-chain systems display gapped state above a critical value of bond alternation parameter, $\delta \approx 0.42$ and up to the fully isolated dimerized limit ($\delta \approx 1$), while showing a gapless behavior below δ of 0.42 down to the uniform chain limit ($\delta \approx 0$) [43,49]. Indeed, the magnitude of spin gap is further enhanced by the frustration between the nearest-neighbor and next-nearest-neighbor exchange couplings [50–52].

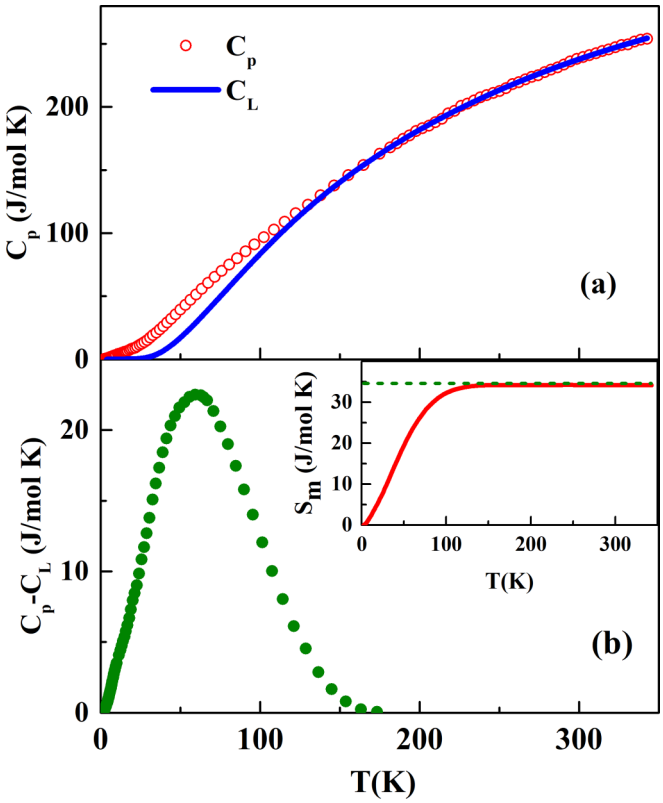

FIG. 4. (a) Temperature dependence of measured heat capacity (C_p) of $Na_2Mn_3O_7$ in the range 1.8–350 K. The solid line represents the lattice contribution (C_L) to the heat capacity, obtained by fitting the experimental C_p data above 150 K with the combined Debye-Einstein model. (b) The magnetic contribution to the heat capacity (C_m) of $Na_2Mn_3O_7$ as a function of temperature. The inset shows the magnetic entropy (S_m) vs temperature, and the dotted line denotes the theoretical value of the entropy ($3R\ln 4$) for an $S = \frac{3}{2}$ system with three magnetic ions per formula unit.

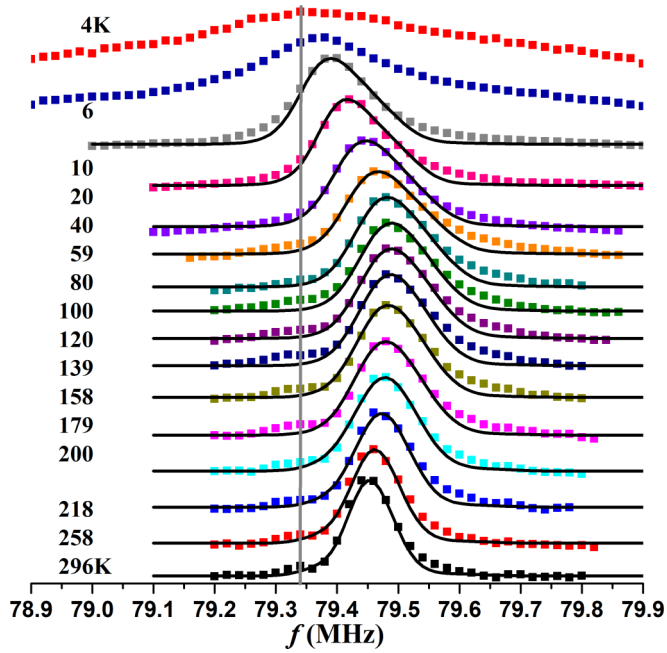

FIG. 5. Frequency variation of ^{23}Na NMR spectra of $Na_2Mn_3O_7$ at different temperatures. Theoretically simulated spectra [Eq. (8)] are shown by the continuous lines. The vertical line represents ^{23}Na reference position.

C. Magnetic heat capacity

The heat capacity of $Na_2Mn_3O_7$ as a function of temperature is shown in Fig. 4(a). C_p decreases monotonically with decrease in temperature. In $C_p(T)$ curve, there is no clear evidence of magnetic ordering of Mn^{4+} moments down to lowest measured temperature 1.8 K, which is consistent with magnetization data. To obtain better information on the nature of magnetic ground state from the heat capacity data, one has to subtract the lattice contribution (C_L) from the measured C_p. We have calculated the lattice contribution by fitting the high-temperature C_p data with the combined Debye-Einstein model and shown in Fig. 4(a). It is clear from the figure that the combined Debye-Einstein model fits the experimental data well down to 150 K. Below 150 K, C_L decreases at a faster rate, as a result, the difference between $C_p(T)$ and $C_L(T)$ curves widens. This behavior suggests a significant magnetic contribution to the heat capacity. Figure 4(b) shows the magnetic contribution to the heat capacity, C_m, obtained after subtracting the lattice contribution from the total heat capacity. The main feature is a broad peak at around 62 K, as expected in an 1D AFM system. Blöte calculated magnetic heat capacity of one-dimensional AFM Heisenberg spin chains for different S between $\frac{1}{2}$ and $\frac{5}{2}$ and observed that C_m vs $2k_BT/JS(S+1)$ plot exhibits a broad peak, which shifts progressively toward lower temperature as S increases from $\frac{1}{2}$ to $\frac{5}{2}$ [53]. For $S = \frac{3}{2}$, the peak in $C_m(T)$ appears at $k_BT/J \sim 2.6$. Comparing our experimental data with this theoretical derivation, one finds $J = 24$ K. The deduced value of J is comparable to that obtained by fitting the high-temperature spin susceptibility with the Bonner-Fisher model. We have also estimated the entropy (S_m) associated with the short-range magnetic correlations. S_m can be obtained by integrating (C_m/T). $S_m(T)$ is shown in the inset of Fig. 4(b). With increase in temperature, S_m increases rapidly and starts to saturate above 130 K. The estimated saturation value of S_m is 34.3 J/mol K, which is very close to the theoretical value of the entropy ($3R\ln 4$) for three Mn^{4+} ions per formula unit with spin $S = \frac{3}{2}$. We have also measured heat capacity in presence of magnetic field up to 9 T. C_p does not show field dependence, indicative of absence of long-range magnetic ordering.

D. NMR spectra and shift

Figure 5 shows the frequency swept ^{23}Na NMR spectra of $Na_2Mn_3O_7$ at various temperatures between 4 and 296 K. Even though there are two different crystallographic sites for Na ion, only one resonance peak is observed at all temperatures. There is clearly a temperature-dependent shift as well as anisotropic magnetic broadening of the spectra. It may be mentioned here that the paramagnetism of defect spins does not affect the shift, though it induces broadening in the spectra that becomes prominent below ~10 K [35,45,54]. ^{23}Na with $I = \frac{3}{2}$ undergoes nuclear quadrupolar interaction in presence of electric field gradient at the nucleus. The spectra are thus

fitted with the following equation of resonance frequencies, which is obtained by considering the magnetic hyperfine interaction and nuclear quadrupolar interaction as first-order perturbations to the Zeeman interaction,

$$\nu(m \rightarrow m-1) = \nu_{\text{ref}}[1 + K_{\text{iso}} + K_{ax}(3\cos^2\theta - 1) + K_{\text{aniso}}\sin^2\theta\cos 2\phi] + \frac{\nu_Q}{2}\left(m - \frac{1}{2}\right) \times[(3\cos^2\theta - 1) + \eta\sin^2\theta\cos 2\phi]. \quad (8)$$

A Lorentzian distribution function with a temperature-dependent linewidth parameter has been used in the deconvolution procedure. The variables obtained in the fitting are the shift parameters K_{iso} and K_{ax} that are plotted against temperature in Fig. 6(a). The parameter K_{iso} increases with decreasing temperature, passes through a broad maximum at around 120 K and decreases rapidly at low temperature. The nature of temperature dependence of K_{iso} is qualitatively similar to that of χ_{spin}. It is found that the temperature independent quadrupolar coupling constant, ν_Q, is ∼150 kHz; and that the shift parameter K_{aniso} and the electric field gradient asymmetry η can be ignored at all temperatures. The rapid decrease of K_{iso} below ∼50 K [Fig. 6(a)] is an indication of a nonmagnetic ground state in $Na_2Mn_3O_7$.

Figure 6(b) shows that isotropic shift K_{iso} has a linear dependence on χ_{spin}. In other words, the temperature dependence of K_{iso} follows that of χ_{spin}. In systems where the probe nuclei experience a transferred hyperfine field arising from localized magnetic moments, K_{iso} is expressed as a sum of a temperature-independent part (K_0) and a temperature-dependent part, which is linear in χ_{spin} due to the localized moments, as given by,

$$K_{\text{iso}} = K_0 + (H_{hf}/N_A\mu_B)\chi_{\text{spin}}(T), \quad (9)$$

where H_{hf} is the hyperfine field at the nucleus, N_A is the Avogadro number and μ_B is the Bohr magneton. The linear fit to the data in Fig. 6(b) with the above equation yields $K_0 \simeq 0.031(\pm 0.004)\%$ and $H_{hf} \simeq 0.49(\pm 0.02)$ kOe. The same fit for K_{iso} vs. T data is shown as thick solid line in Fig. 6(a).

Below 50 K, the experimental data of K_{iso} can be fitted with an equation similar to Eq. (7),

$$K_{\text{iso}}(\%) = K_0 + 1.5T^{-0.5}\exp(-\Delta_0/k_BT). \quad (10)$$

The fitting is shown in Fig. 6(c). The value of Δ_0 thus obtained is 25 ± 1 K, which agrees well with the gap deduced from the low-temperature χ_{spin} data. However, as mentioned earlier that K_{iso} is not affected by the presence of impurity spins, the value of gap determined from NMR shift measurements is perhaps more reliable than that obtained from magnetic measurements.

It is possible to estimate Δ from J for alternating spin-chain systems with $S = \frac{1}{2}$ when the ratio between nearest-neighbor and next-nearest-neighbor exchange interactions in a spin chain is known [11,55]. A relation between Δ and J also exists for two-dimensional system with $S = \frac{1}{2}$ [56]. For an isotropic $S = 1$ infinite chain (Haldane chain), Δ/J is 0.41 [57,58]. This relation holds good in $S = \frac{1}{2}$ ladder systems where there is AFM coupling between spins along the chain and a large FM transverse coupling [59]. No such relationship has been found so far for any low-dimensional system with $S = \frac{3}{2}$.

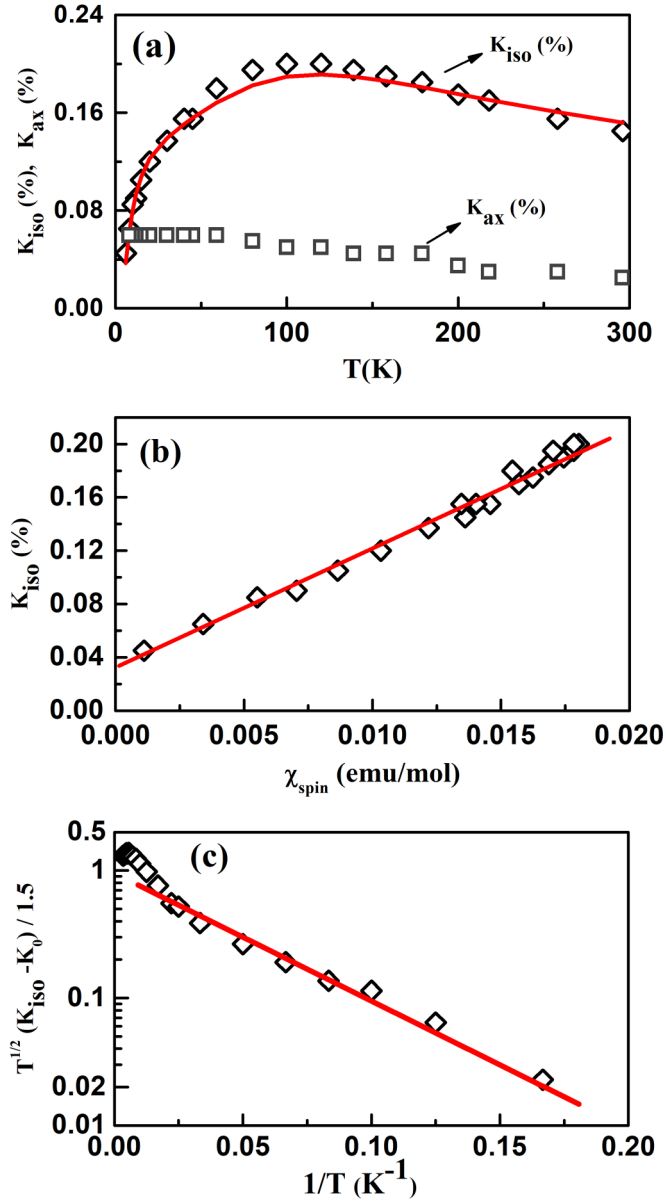

FIG. 6. (a) Temperature dependence of K_{ax} (□) and K_{iso} (◊) of $Na_2Mn_3O_7$; the solid line is fit of K_{iso} with Eq. (9). (b) The plot of K_{iso} vs. χ_{spin} and the solid line is the linear fit. (c) The plot of $2/3[K_{\text{iso}} - K_0]T^{1/2}$ vs. inverse of temperature for $T \leqslant 300$ K; and the fit of the data (solid line) in between 6–60 K with the activation relation Eq. (10).

E. Nuclear spin-lattice relaxation rate

Spin-lattice relaxation time (T_1) has been studied by exciting the spectrum around the peak position using an appropriate 90° radio-frequency pulse in standard solid-echo pulse sequence 90°-τ-90°-echo, where τ is the variable delay time during which nuclear magnetization evolves to $M(\tau)$ on its way to thermal equilibrium value M_0 following the initial 90° pulse. T_1 is estimated by fitting $M(\tau)$ with the equation for the

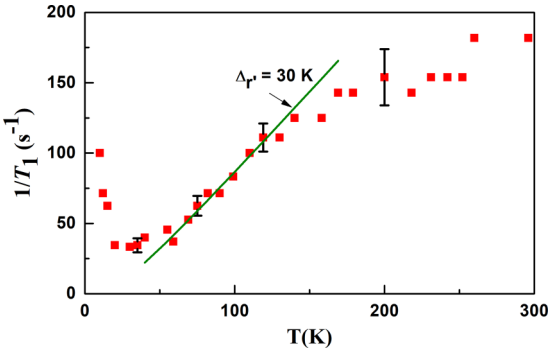

FIG. 7. Temperature dependence of ^{23}Na nuclear spin-lattice relaxation rate, $1/T_1$, in $Na_2Mn_3O_7$, and its fit to $T_1^{-1} \propto T\exp(-\Delta_r/k_BT)$. As the temperature is decreased below ~25 K, an increasingly faster relaxation induced by the defect spins, as described in Sec. III B, dominates the relaxation process.

central transition of ^{23}Na spectrum (spin $I = \frac{3}{2}$),

$$1 - M(\tau)/M_0 = C_1[0.1\exp(-\tau/T_1) + 0.9\exp(-6\tau/T_1)]. \quad (11)$$

In the above equation, C_1 and T_1 are the fitting parameters. Figure 7 shows the temperature dependence of spin-lattice relaxation rate $(1/T_1)$. With decrease in temperature, $(1/T_1)$ decreases down to 25 K, below which $(1/T_1)$ increases. The relaxation behavior is typical of low-dimensional spin systems and the increase in $1/T_1$ at low temperature is attributed to impurity spins [33,54]. We have already discussed that the spin arrangement in $Na_2Mn_3O_7$ is very similar to those in quasi-one-dimensional system. Often, low-dimensional compounds and spin ladders that are made of simultaneous strong and relatively weak couplings among magnetic ions show activated temperature dependence of spin-lattice relaxation rate [33,34,44,45,60].

There are spin-ladder systems, which demonstrate magnetic field-induced quantum critical behavior where spin excitations evolve from magnons in the gapped Bose-Einstein condensate (BEC) state at low field to spinons in the gapless Tomonaga-Luttinger-liquid state at high field [44,60]. In the intermediate field regime, T_1^{-1} exhibits a pronounced and continuous variation, which is shown to scale in accordance with quantum criticality. The temperature dependence of T_1^{-1} in such systems can be explained more appropriately using the expression [60],

$$T_1^{-1} \propto T^{\alpha}\exp(-\Delta_{r'}/k_BT); \quad \Delta_{r'} = g\mu_B(H_c - H), \quad (12)$$

where H_c is the critical field at which the singlet-triplet gap disappears, g is the Landé g factor, and H is the applied magnetic field. The exponent α depends on the effective dimension of the magnon dispersion as selected by thermal fluctuations. It has a high value of 2 at very low temperature where the interchain coupling becomes effective. On increasing the temperature, α gradually decreases and becomes 0 at high temperature. For $H < H_c$, and temperature in the gapped region, α has been shown to be close to 1 [60]. The temperature dependence of spin-lattice relaxation rate in alternating spin-1/2 chain compounds $AgVOAsO_4$ and $NaVOAsO_4$ is observed to follow the above expression [44,45]. For these compounds, T_1^{-1} shows an activated temperature dependence below 11 K with α close to 2, i.e., the spin-lattice relaxation in the low-temperature region is dominated by 3D spin correlations. Due to the upturn in $T_1^{-1}(T)$ curve below 25 K, we are unable to determine the nature of spin correlations in $Na_2Mn_3O_7$ at low temperature. However, the relaxation data in the temperature region 50 K $< T <$ 120 K can be fitted with Eq. (12) for $\alpha = 1$, as shown in Fig. 7. The fit yields $\Delta_{r'} = 30$ K, which is in reasonable agreement with the spin gap obtained from NMR shift. It may be mentioned here that we have also tried to fit the experimental data for $\alpha < 1$. With the decrease in α below 1, $\Delta_{r'}$ is found to increase monotonically and the quality of fit becomes inferior. Incidentally, the observed value of $\Delta_{r'}$ corresponds to H_c of ~15 T, that may be compared with H_c of ~10 T in $AgVOAsO_4$ [44]. Different behavior of T_1^{-1} is expected depending upon whether H is set below or above H_c, and a further confirmation of BEC behavior would have been possible if T_1^{-1} could be measured at higher magnetic fields [60].

IV. CONCLUSION

We have studied the magnetic properties of a maple-leaf lattice antiferromagnetic compound $Na_2Mn_3O_7$ using magnetic susceptibility and heat capacity, and also the microscopic technique of NMR spectroscopy. The results indicate that this compound possesses a nonmagnetic ground state with an energy gap of 25–28 K in its spin excitation spectrum. Moreover, the nuclear spin-lattice relaxation behavior seems to indicate that the studied compound could be a candidate for Bose-Einstein condensate. High field magnetization measurements and neutron diffraction study would be useful for further elucidation of magnetic properties of this compound.

ACKNOWLEDGMENTS

We thank C. Dasgupta for useful discussion. The work was supported by Dept. of Atomic Energy (DAE), Govt. of India. V.G. acknowledges UGC-DAE CSR for LTHM facilities. C.V. acknowledges SERB, Govt. of India for funding through National Post Doctoral Fellowship (PDF/2017/002462).

[1] F. D. M. Haldane, Phys. Rev. Lett. **50**, 1153 (1983).
[2] R. Claessen, M. Sing, U. Schwingenschlögl, P. Blaha, M. Dressel, and C. S. Jacobsen, Phys. Rev. Lett. **88**, 096402 (2002).
[3] A. J. Daley, H. Pichler, J. Schachenmayer, and P. Zoller, Phys. Rev. Lett. **109**, 020505 (2012).
[4] M. Imada, A. Fujimori, and Y. Tokura, Rev. Mod. Phys. **70**, 1039 (1998).
[5] X. Zotos, F. Naef, and P. Prelovšek, Phys. Rev. B **55**, 11029 (1997).
[6] A. V. Sologubenko, E. Felder, K. Giannó, H. R. Ott, A. Vietkine, and A. Revcolevschi, Phys. Rev. B **62**, R6108 (2000).

[7] H. Katsura, N. Nagaosa, and P. A. Lee, Phys. Rev. Lett. **104**, 066403 (2010).

[8] A. N. Vasilev, M. M. Markina, and E. A. Popova, Low Temp. Phys. **31**, 203 (2005).

[9] J. C. Bonner and M. E. Fisher, Phys. Rev. **135**, A640 (1964).

[10] S. Eggert, I. Affleck, and M. Takahashi, Phys. Rev. Lett. **73**, 332 (1994).

[11] D. C. Johnston, R. K. Kremer, M. Troyer, X. Wang, A. Klümper, S. L. Budko, A. F. Panchula, and P. C. Canfield, Phys. Rev. B **61**, 9558 (2000).

[12] A. Klümper and D. C. Johnston, Phys. Rev. Lett. **84**, 4701 (2000).

[13] D. Hone and A. Pires, Phys. Rev. B **15**, 323 (1977).

[14] H. Lu, T. Yamamoto, W. Yoshimune, N. Hayashi, Y. Kobayashi, Y. Ajiro, and H. Kageyama, J. Am. Chem. Soc. **137**, 9804 (2015).

[15] L. D. Sanjeewa, V. O. Garlea, M. A. McGuire, C. D. McMillen, H. Cao, and J. W. Kolis, Phys. Rev. B **93**, 224407 (2016).

[16] G. R. Wagner and S. A. Friedberg, Phys. Lett. **9**, 11 (1964).

[17] R. Dingle, M. E. Lines, and S. L. Holt, Phys. Rev. **187**, 643 (1969).

[18] M. Niel, C. Cros, G. Le Flem, M. Pouchard, and P. Hagenmuller, Physica B **86–88**, 702 (1977).

[19] H. Mutka, C. Payen, and P. Molini, Europhys. Lett. **21**, 623 (1993).

[20] G. E. Granroth, M. W. Meisel, M. Chaparala, Th. Jolicœur, B. H. Ward, and D. R. Talham, Phys. Rev. Lett. **77**, 1616 (1996).

[21] A. B. Christian, A. Rebello, M. G. Smith, and J. J. Neumeier, Phys. Rev. B **92**, 174425 (2015).

[22] S. Itoh, Y. Endoh, K. Kakurai, H. Tanaka, S. M. Bennington, T. G. Perring, K. Ohoyama, M. J. Harris, K. Nakajima, and C. D. Frost, Phys. Rev. B **59**, 14406 (1999).

[23] M. Hase, M. Soda, T. Masuda, D. Kawana, T. Yokoo, S. Itoh, A. Matsuo, K. Kindo, and M. Kohno, Phys. Rev. B **90**, 024416 (2014).

[24] B. Song, M. Tang, E. Hu, E. Hu, O. J. Borkiewicz, K. M. Wiaderek, Y. Zhang, N. D. Phillip, X. Liu, Z. Shadike, C. Li, L. Song, Y.-Y. Hu, M. Chi, G. M. Veith, X.-Q. Yang, J. Liu, J. Nanda, K. Page, and A. Huq, Chem. Mater. **31**, 3756 (2019)

[25] E. Adamczyk and V. Pralong, Chem. Mater. **29**, 4645 (2017).

[26] Q. Wang, W. Yang, F. Kang, and B. Li, Energy Storage Mater. **14**, 361 (2018).

[27] K. Sada, B. Senthilkumar, and P. Barpanda, ACS Appl. Energy Mater. **1**, 6719 (2018).

[28] F. M. Chang and M. Jansen, Anorg. Allg. Chem. **531**, 177 (1985).

[29] D. Schmalfuß, P. Tomczak, J. Schulenburg, and J. Richter, Phys. Rev. B **65**, 224405 (2002).

[30] Y. Haraguchi, A. Matsuo, K. Kindo, and Z. Hiroi, Phys. Rev. B **98**, 064412 (2018).

[31] C. Masquelier, M. Tabuchi, K. Ado, R. Kanno, Y. Kobayashi, Y. Maki, O. Nakamura, and J. B. Goodenough, J. Solid State Chem. **123**, 255 (1996).

[32] R. Alcántara, M. Jaraba, P. Lavela, J. L. Tirado, E. Zhecheva, and R. Stoyanova, Chem. Mater. **16**, 1573 (2004).

[33] S. Taniguchi, T. Nishikawa, Y. Yasui, Y. Kobayashi, M. Sato, T. Nishioka, M. Kontani, and K. Sano, J. Phys. Soc. Jpn. **64**, 2758 (1995).

[34] H. Iwase, M. Isobe, Y. Ueda, and H. Yasuoka, J. Phys. Soc. Jpn. **65**, 2397 (1996).

[35] K. Ghoshray, B. Pahari, B. Bandyopadhyay, R. Sarkar, and A. Ghoshray, Phys. Rev. B **71**, 214401 (2005).

[36] B. Pahari, K. Ghoshray, R. Sarkar, B. Bandyopadhyay, and A. Ghoshray, Phys. Rev. B **73**, 012407 (2006).

[37] Y. Uchiyama, Y. Sasago, I. Tsukada, K. Uchinokura, A. Zheludev, T. Hayashi, N. Miura, and P. Böni, Phys. Rev. Lett. **83**, 632 (1999).

[38] A. A. Tsirlin, R. Nath, J. Sichelschmidt, Y. Skourski, C. Geibel, and H. Rosner, Phys. Rev. B **83**, 144412 (2011).

[39] L. de Jongh and A. Miedema, Adv. Phys. **23**, 1 (1974).

[40] S. Sachdev and K. Damle, Phys. Rev. Lett. **78**, 943 (1997).

[41] K. Damle and S. Sachdev, Phys. Rev. B **57**, 8307 (1998).

[42] K. Hallberg, X. Q. G. Wang, P. Horsch, and A. Moreo, Phys. Rev. Lett. **76**, 4955 (1996).

[43] M. Yajima and M. Takahashi, J. Phys. Soc. Jpn. **65**, 39 (1996).

[44] N. Ahmed, P. Khuntia, K. M. Ranjith, H. Rosner, M. Baenitz, A. A. Tsirlin, and R. Nath, Phys. Rev. B **96**, 224423 (2017).

[45] U. Arjun, K. M. Ranjith, B. Koo, J. Sichelschmidt, Y. Skourski, M. Baenitz, A. A. Tsirlin, and R. Nath, Phys. Rev. B **99**, 014421 (2019).

[46] F. Hammerath, E. M. Brüning, S. Sanna, Y. Utz, N. S. Beesetty, R. Saint-Martin, A. Revcolevschi, C. Hess, B. Büchner, and H.-J. Grafe, Phys. Rev. B **89**, 184410 (2014).

[47] F. Hammerath, S. Nishimoto, H. J. Grafe, A. U. B. Wolter, V. Kataev, P. Ribeiro, C. Hess, S. L. Drechsler, and B. Büchner, Phys. Rev. Lett. **107**, 017203 (2011).

[48] S.-H. Baek, K.-Y. Choi, H. Berger, B. Büchner, and H.-J. Grafe, Phys. Rev. B **86**, 180405(R) (2012).

[49] S. Yamamoto, Phys. Rev. B **55**, 3603 (1997).

[50] R. Roth and U. Schollwöck, Phys. Rev. B **58**, 9264 (1998).

[51] T. Hikihara, M. Kaburagi, and H. Kawamura, Phys. Rev. B **63**, 174430 (2001).

[52] S. Watanabe and H. Yokoyama, J. Phys. Soc. Jpn. **68**, 2073 (1999).

[53] H. W. J. Blöte, Physica **78**, 302 (1974).

[54] R. Nath, A. V. Mahajan, N. Büttgen, C. Kegler, A. Loidl, and J. Bobroff, Phys. Rev. B **71**, 174436 (2005).

[55] T. Barnes, J. Riera, and D. A. Tennant, Phys. Rev. B **59**, 11384 (1999).

[56] S. Miyahara and K. Ueda, Phys. Rev. Lett. **82**, 3701 (1999).

[57] R. Botet, R. Jullien, and M. Kolb, Phys. Rev. B **28**, 3914 (1983).

[58] M. P. Nightingale and H. W. J. Blöte, Phys. Rev. B **33**, 659 (1986).

[59] S. Larochelle and M. Greven, Phys. Rev. B **69**, 092408 (2004).

[60] S. Mukhopadhyay, M. Klanjšek, M. S. Grbić, R. Blinder, H. Mayaffre, C. Berthier, M. Horvatić, M. A. Continentino, A. Paduan-Filho, B. Chiari, and O. Piovesana, Phys. Rev. Lett. **109**, 177206 (2012).